

**Amorphous silicon based photovoltaics
--- from earth to the "final frontier"**

Jeffrey Yang, Arindam Banerjee, and Subhendu Guha

United Solar Systems Corp.
1100 West Maple Road
Troy, Michigan 48084 USA
Fax: (248) 362-4442
email: jyang@uni-solar.com

Abstract

We highlight the advances made in amorphous silicon alloy photovoltaic technology leading to large-scale commercial deployment. The paper discusses multijunction devices made on lightweight flexible substrates; various aspects of attaining high efficiency devices are described. The eminent role of the roll-to-roll continuous deposition technique in propelling the technology to global market is elucidated. The logical emergence of this technology as a lightweight solar-power generator for extraterrestrial application is discussed. Results of high specific power under space conditions are presented. The future of the technology in terms of both device efficiency and product efficacy are given.

1. Introduction

The last quarter century witnessed the birth, the adolescence, and the maturity of amorphous silicon (a-Si) based photovoltaic (PV) technology. As we usher in the twenty-first century, we must also meet the ever-increasing energy demand while addressing environmental issues and ecological concerns. a-Si PV technology has positioned itself as the low-cost solution to the challenge of energy, environmental, and ecology -- the e-tripos. As the a-Si PV industry still experiences unavoidable growing pains, large-volume manufacturing plants are ready to demonstrate their competitiveness in the rapidly growing global market. PV in general, and a-Si technology in particular, will undoubtedly play a significant role in providing clean, quiet, and renewable energy harvested from the inexhaustible sun. The two billion plus people on earth who have no ready access to electricity await solar energy to brighten their lives. The volume of worldwide sales of a-Si PV modules was 34 MW in 2001, a phenomenal growth of 26% over the previous year, but only represents less than 10% of the total PV market. In the next quarter century, we expect the a-Si technology to attain a greater share of the world market.

In this paper, we shall first briefly review the advantages of a-Si PV technology, placing emphasis on multijunction structures. We shall limit our discussion to solar cells deposited on flexible substrates. Solar cells made on glass superstrates will not be discussed here. We shall then touch upon the essence of the roll-to-roll manufacturing process and the advantages of solar panels on flexible substrates. Examples of terrestrial products will be given. In recent years, the feasibility of using a-Si PV for space applications has been investigated due to its high specific power (W/kg) and low cost. Nineteen months and 252 million miles of invaluable experience on board MIR Space Station has revolutionarily uplifted our outlook for use of a-Si solar arrays for future missions in space. a-Si PV has been identified as the enabling technology for certain applications. We shall describe the advantages of a-Si PV for non-terrestrial applications. Although a-Si PV technology is advancing rapidly, many challenges still remain. We shall highlight directions for future research effort.

2. Advantages of a-Si based multijunction structures

2.1 *a-Si based materials*

Low cost is one of the leading advantages of a-Si PV. Two of the major ingredients of the a-Si alloy are silicon and hydrogen. They are environmentally friendly and abundant on earth. Furthermore, a-Si alloys are characterized by a high absorption coefficient. Only a thin film ($< 1 \mu\text{m}$) is needed to absorb the sunlight, and this leads to low material cost. Good conversion efficiency is another advantage for a-Si PV. In the laboratory, we use the radio-frequency plasma-enhanced chemical vapor deposition method and have demonstrated a stable cell efficiency of 13% using a spectrum-splitting triple-junction structure

[1]. In addition, low cost manufacturing is also an important requirement. The roll-to-roll continuous deposition process pioneered by Energy Conversion Devices, Inc. [2] has now entered into its eighth generation and incorporates state-of-the-art design and in-line diagnostic sensors [3].

2.2 Multijunction approach

While disorder leads to a high absorption coefficient for a-Si alloys, it also creates wide band tails in the energy gap. The band tails and other structural defects in the form of weak, dangling, and strained bonds affect transport of carriers in the solar cell. Furthermore, a-Si alloys degrade upon light soaking due to the Staebler-Wronski effect (SWE) [4]. To alleviate these problems, the multijunction approach [5], where more than one cell is deposited on top of another, is used. This approach allows one to use thinner cells to minimize the SWE. In addition, the multijunction structure incorporates materials with different band gaps that increase the overall spectral response of the device and results in higher efficiency. We shall next discuss the multijunction structures.

Figure 1 illustrates four solar cell structures that we have investigated in our laboratory. In all four structures, we use thin stainless steel (SS) substrates, which were first coated with textured silver (Ag) and zinc oxide (ZnO) back reflectors to facilitate light trapping for enhancing the short-circuit current density (J_{sc}) of the solar cell. The effect of light trapping will be discussed later.

Figure 1 (a) shows the basic single-junction structure, where the intrinsic (i) layer is a hydrogenated a-Si alloy (a-Si:H) with a typical optical band gap of 1.75 eV. The limitation of this structure is its stabilized efficiency. In order to achieve high initial efficiencies, one would usually increase the thickness of the i layer. However, a thick i layer results in a weak internal electric field, and the solar cell suffers from significant degradation due to the SWE. Nevertheless, this structure is commonly used to evaluate solar cell performance prepared by different materials, device designs, and deposition conditions.

Figure 1 (b) shows the basic double-junction structure, where we use only a-Si:H without any band gap modifying material. The major advantage of this structure is that the top and bottom component cells can be made thin to minimize the SWE. While the current in such a solar cell is smaller than the single junction a-Si:H cell, the fill factor (FF) is usually higher, and the open-circuit voltage (V_{oc}) is nearly twice the single-junction value [6]. The stabilized efficiency of the double-junction cells is in general higher than the single-junction a-Si:H cells.

One way to improve the double-junction cell efficiency is to broaden the spectral response of the absorber layer. By incorporating germanium (Ge) into the bottom cell, one can reduce the band gap and enhance the long wavelength response. However, the carrier transport properties of the a-SiGe:H materials are inferior to those of the a-Si:H material. In general, a-SiGe:H solar cells exhibit lower V_{oc}

and poorer FF than the a-Si:H cells of similar thickness. On the other hand, the enhancement in J_{sc} can more than overcome the reduction in V_{oc} and FF, especially when one uses novel device designs such as those to be discussed later. For an a-Si:H/a-SiGe:H dual band gap configuration like that shown in Fig. 1 (c), the top cell needs to be thicker than that in Fig. 1 (b) to produce higher current. Although V_{oc} and FF are usually lower in the dual gap structure, the efficiency is higher due to the higher J_{sc} [7]. Since the top cell needs to be sufficiently thick to produce a current large enough to match the current from the low band gap bottom cell, it is also more susceptible to the SWE. This leads to the design of Fig. 1 (d), where one uses a triple-junction approach [8]. In this structure, the top cell is a-Si:H with band gap of ~ 1.75 eV to absorb the blue photons, the middle cell uses a-SiGe:H with $\sim 15\%$ Ge to capture the green photons, and the bottom cell incorporates $\sim 30\%$ Ge to absorb the red photons. The textured back reflector at the bottom and the indium tin oxide (ITO) antireflection coating on the top complete the most efficient cell structure to date. Key elements for achieving efficient multijunction cells are described below.

2.3 Back reflector

A highly reflective metal, such as Al or Ag, is usually deposited on top of SS to enhance its reflectivity. The most effective reflector we have used to date consists of a two-layer structure [9]. It contains a textured Ag layer followed by a conductive ZnO layer to form the back reflector (BR) and facilitate light trapping in the solar cell. To illustrate the effect of the BR, we compare quantum efficiency curves for two a-SiGe:H cells in Fig. 2. They were deposited using identical conditions, except that one was on SS and the other on Ag/ZnO. An enhancement in J_{sc} from 17.3 mA/cm^2 to 23.7 mA/cm^2 is achieved. In fact, for a multijunction cell, the quality of the bottom cell and the quality of the BR dictate the J_{sc} of the bottom cell, which in turn governs the J_{sc} of the multijunction cell.

2.4 Current matching

To achieve high performance multijunction cells, one must first consider the thickness and band gap of the component cells. For a double-junction structure, one should first evaluate the capability of the bottom cell on BR and see how much current it can generate under the standard AM1.5 spectrum. The rule of thumb is then to design the top cell to produce about half the current. During the optimization process, it is often useful to evaluate the bottom cell with a red filter to simulate its operation in a double-junction structure. The corresponding top cell should be optimized under the AM1.5 illumination.

Since the top cell usually uses a-Si:H and shows a good FF due to its small thickness and superior material quality, it is beneficial to slightly limit the double-junction current by the top cell. It is also important to keep in mind that the desired amount of current mismatch should be determined by the degradation behavior of the component cells after light soaking. A similar approach can be

applied to the triple-junction structure. One should first evaluate the bottom cell on BR. The top cell should roughly produce one-third of the bottom-cell current, and the middle cell two thirds. Again, it is useful to evaluate the middle and bottom cells with appropriate filters to simulate their operations in a triple-junction structure [10].

2.5 *Doped layers and tunnel junctions*

The doped layers that flank the *i* layers are necessary for solar cell operations, but they are not photovoltaically active. They represent parasitic loss both electrically and optically. The *p* layer through which the light enters the solar cell is particularly important and should be as transparent and conductive as possible. We have developed a microcrystalline *p* layer, which resulted in a significant improvement in the cell performance [11]. In a multijunction structure, a tunnel-junction is formed consisting of the two adjacent doped layers of the two adjacent component cells. Because the tunnel junction consists of thin doped layers, carriers can be considered to 'tunnel' through the layers. In reality, photogenerated electrons and holes recombine in the 'tunnel' junction. Thus, it is also referred to as the 'recombination' junction. However, the polarity of the tunnel junction is opposite to that of the multijunction device. It is therefore important to minimize losses associated with the tunnel-junction [12]. Table 1 compares characteristics of a-Si:H/a-Si:H double-junction cells with two different tunnel-junction configurations. One notes that a superior tunnel-junction leads to a higher cell efficiency [1].

2.6 *Component cells*

The quality of the component cells determines the performance of the multijunction structure [13]. The component cells are the basic building blocks. It is convenient to evaluate and optimize each component cell separately, then integrate them into a multijunction configuration. It is useful to evaluate the component cells under appropriate illumination conditions corresponding to their respective spectral response in a multijunction structure. In a spectrum-splitting triple-junction structure, the top cell receives the full sunlight, and should be evaluated under AM1.5. The middle cell receives full sunlight less the amount absorbed by the top cell. In addition, the middle cell does not receive much optical enhancement from the BR. We often deposit the middle cell on bare SS, and evaluate its performance with a $\lambda > 530$ nm filter. The bottom cell enjoys full benefit from the BR, and is typically measured using a $\lambda > 630$ nm filter.

Optimization of the component cells requires a major effort. We should point out that high quality component cells are necessary but not sufficient conditions for achieving high efficiencies. This is analogous to the fact that high quality intrinsic material is a necessary but not sufficient condition for fabricating high efficiency solar cells.

For the top cell, we use a-Si:H with a band gap of ~ 1.75 eV. To achieve 8 to 9 mA/cm² in a high efficiency triple-junction structure, one would need an *i* layer ~ 2000 Å thick. Hydrogen dilution during film growth, first suggested by Guha et al. in 1981 [14], is now widely used to obtain high quality a-Si:H *i* layers [15]. The best top cell performance is obtained using a hydrogen dilution value near the amorphous-to-microcrystalline transition [6]. This effect will be reviewed in more detail in this volume [16].

For the middle and bottom cells, we use a-SiGe:H alloys with $\sim 15\%$ Ge and $\sim 30\%$ Ge in the absorber layers, corresponding to band gaps of ~ 1.6 and 1.45 eV, respectively. In general, carrier transport properties are inferior in a-SiGe:H compared to a-Si:H. To overcome this difficulty, a novel cell design was developed [17]. Rather than a constant band gap such as one normally makes, this novel design employs band gap profiling by varying the Si to Ge ratio throughout the intrinsic layer. A Ge rich region, corresponding to a narrower band gap, is deposited near the *p* layer [18]. This design helps the low mobility holes so that, on the average, they only need to traverse a short distance to reach the *p* layer. On the other hand, electrons, which possess higher mobility, would not have much difficulty to traverse the *i* layer and arrive at the *n* layer. A Si rich region is incorporated at the *p/i* interface to improve the interface properties and to achieve higher V_{oc} .

The bottom cell receives full benefit from the BR, and thus it can be made relatively thin while still generating sufficient current. The middle cell, on the other hand, needs to be thick enough to generate sufficient current without suffering much from the SWE. Hydrogen dilution has also been reported to improve the middle and bottom cell performance [19]. Table 2 summarizes the best stabilized component cell efficiencies achieved in our laboratory that led to the stable 13% world record triple-junction cell efficiency [1].

2.7 Light soaking effect

The SWE significantly impacts the performance of a-Si alloy solar cells [20]. To mitigate the problem, one resorts to three fundamental measures. One is to improve the material quality, such as using hydrogen dilution during film growth. Another is to incorporate a novel device design, such as the band gap profiling scheme in a-SiGe:H solar cells. The third is to use the multijunction approach discussed above. We have investigated the four structures shown in Fig. 1 and studied their stability against light soaking. Table 3 summarizes the best stabilized efficiency for each structure. It is noted that the a-Si:H single cell has the lowest stable efficiency. The a-Si:H/a-Si:H double-junction structure improves the stable efficiency to over 10%. Replacement of a-Si:H by a-SiGe:H in the bottom cell further improves the stabilized efficiency to 12.4% [13]. The most efficient configuration is the spectrum-splitting triple-junction structure showing a world record stabilized efficiency of 13% [1].

The AM1.5 J-V characteristics of the record cell show an initial efficiency of 14.6%. The J-V and the corresponding quantum efficiency plot are shown in Figs. 3 (a) and 3 (b), respectively. From Fig. 3 (b), one notes that the spectral response spans from 350 nm to beyond 950 nm. The spectrum-splitting feature is reflected by the spectral response of the top, middle, and bottom component cells. One also notes a current mismatch of ~ 0.5 mA/cm² between adjacent component cells, with the top cell being the current limiting cell. Since the triple-junction structure shows the best performance for small area cells and large area modules in the laboratory [21], we decided to use the structure in our large-volume manufacturing plant.

3. Manufacturing technology and down-to-earth applications

3.1 Manufacturing technology

A key feature in our manufacturing technology is the roll-to-roll continuous deposition process. Only flexible substrates are compatible with this process. A roll of 5-mil thick SS substrate goes through four consecutive roll-to-roll machines first to wash, and then to deposit the BR, triple-junction structure, and top conductive layer [22]. While the width of the SS rolls used is 14", there is no constraint on the length of the roll. After the four roll-to-roll processes, the coated web is then cut into a predetermined size for module fabrication. Figure 4 illustrates the roll-to-roll triple-junction deposition scheme. Details of this process and state-of-the-art key features of our most advanced 30 MW annual capacity a-Si processor will be described by Izu and Ellison [3] in this volume.

3.2 Module fabrication process

After the roll of coated web is cut to the desired size, the remaining module fabrication processes are carried out as illustrated by the block diagram in Fig. 5. Quality assurance and control are rigorously instituted, while the proprietary short passivation process assures high process yield. Details of the module fabrication process have been given elsewhere [23].

3.3 Rigid, flexible, and building integrated products for terrestrial applications

A variety of United Solar products are available in the market, ranging from 3 W to 128 W [24]. They can be generally divided into three categories: rigid, flexible, and building-integrated. The rigid module has a frame around the border and is used for both large-scale power generation and battery charging applications. The flexible modules are for recreational vehicles, sailboats, and foldable battery chargers (see Fig. 6). Esthetically pleasing building integrated applications have become popular and take full advantage of the lightweight and flexible features of our products. An example is shown in Fig. 7. PV laminates with a Peel and Stick feature [25] can be easily bonded to a variety of commercial metal roofs. In this design, the release paper at the back of the laminate can be

easily peeled off and the PV laminate, typically 16 inches wide and 18 feet long, pressed to the front surface of a clean metal roofing panel. The SmartRoofSM system is available to residential home owners as a total solution package. More and more applications are being offered to the growing market.

4. Advantages of United Solar's triple-junction solar cells for space applications

There is an emerging need for lightweight solar arrays on flexible substrates for satellite and airship applications. The development of rugged thin film solar cells with high specific power on lightweight flexible substrates is an enabling technology for such applications. In many cases, low cost is also an important criterion. Current high-efficiency crystalline space solar cells cannot satisfy the three key requirements of (1) high specific power, (2) mechanically rugged properties, and (3) low cost. Typical specific power for the crystalline cells is <100 W/kg. The panels are fragile and need a heavy and fragile cover glass. The solar array cost is high, at ~\$500-\$2000/watt. In contrast, United Solar's a-Si triple-junction solar cells on flexible substrates address all these issues. The specific power is high since (1) the cells are very thin and (2) the substrates are flexible and lightweight. The cells are rugged mechanically since there is no breakable part. The cost is potentially an order of magnitude lower.

4.1 Space qualification tests and the MIR experience

In addition to the high specific power, mechanical ruggedness, and low cost that United Solar's triple-junction solar cells can offer, certain space qualification tests have also shown promising results. For example, the temperature coefficient for high efficiency triple-junction a-Si alloy cells has been found to be between -0.2 and -0.3% / $^{\circ}\text{C}$, which is superior to crystalline Si devices for high temperature operation. In addition, United Solar's triple-junction cells on SS have been subjected to proton and electron irradiations of various energies and fluences [26, 27]. It has been found that defects that are created by irradiation can be annealed out and cell efficiency restored at the prevailing temperature of ~ 70 $^{\circ}\text{C}$ in orbit [27]. Furthermore, a-Si alloy triple-junction solar cells bonded to an appropriate substrate structure have been subjected to $+150$ $^{\circ}\text{C}$ to -110 $^{\circ}\text{C}$ thermal cycles at 80 $^{\circ}\text{C}$ / min. No change in cell performance was detected.

A real life test was carried out on board the MIR Space Station. Modules fabricated from triple-junction cells interconnected by KVANT of Russia were placed on board the MIR Space Station. Cell data was sent by telemetry, and minimal (virtually no) change in performance was detected during the 19 months and 252 million miles flown in 1998 – 2000 [28].

4.2 AM0 efficiency

The AM0 spectrum is much richer in the blue wavelength region than the AM1.5 spectrum prevalent on the earth. The thickness and band gap of the component cells are reoptimized for the AM0 spectrum. We have demonstrated a total area beginning-of-life efficiency of 12% measured by NASA [26].

4.3 *Flexible substrates*

Two different approaches have been taken for substrate selection. In the first approach, where SS is used, the roll-to-roll production technology has been used to make the solar cells, and the cells are fabricated using the terrestrial production technology, as discussed earlier. The substrate is, however, less than one mil thick, and the cells are optimized for the AM0 spectrum. Typical beginning-of-life efficiency for the cells from the production line is 8.5%. The corresponding value for R & D cells with an area of 460 cm² is 9.5%, as confirmed by NASA Glenn Research Center [29].

In the second approach, we use a one-mil-thick polyimide substrate. The cells on polyimide are at an initial stage of development, but have already shown promising results. NASA Glenn has measured cells with 412 cm² area at 9% beginning-of-life efficiency [30].

4.4 *Specific power*

The advantage of using the SS substrate is that the production technology exists, and we can readily meet the volume demand. The specific power for a triple-junction cell on thin SS has exceeded 350 W/kg. Future work is aimed at improving the initial efficiency to 11% and increasing the specific power to over 750 W/kg. For cells on polyimide, the advantage is higher specific power. We have achieved a specific power exceeding 1250 W/kg (see Fig. 8). With further research, we believe a goal of 2000 W/kg is achievable.

5. **Future directions**

Over the last quarter century, although a-Si PV technology has emerged as a strong contender for providing quiet, clean, and renewable energy for terrestrial applications, many challenges remain, as described below.

5.1 *Cell efficiency*

The fundamental limitation in the solar cell efficiency is in the material quality. Hydrogen dilution during film growth has been effective in improving the material quality and cell stability. Further improvement in a-SiGe:H alloy can benefit the multijunction structure. Innovative cell design and improvement in the BR and ITO can also have significant impact on the cell efficiency.

5.2 *Cell stability*

Improvement in fundamental understanding of the SWE may shine additional light on ways to minimize or eliminate the degradation mechanism. Studying the correlation of the SWE and other properties such as micro-structural change should be helpful.

5.3 *Module cost*

Improvement in manufacturing technology can greatly impact the module cost. Cost reduction in raw material, such as higher throughput without sacrificing the efficiency is a major issue. Use of inexpensive raw materials, encapsulation materials and processes, as well as automation for large-volume production can also significantly reduce manufacturing cost.

5.4 *Space deployment*

A cell interconnect technique, size, weight, specific power of solar arrays, and comprehensive space qualification tests are all important topics and need to be addressed in more detail. A mission to qualify a-Si PV technology in space would be most beneficial.

6. **Summary**

In summary, we have reviewed the advances made in a-Si PV technology that led to the achievement of an AM1.5 13% stable cell efficiency and set the foundation for the spectrum splitting triple-junction structure being manufactured by the roll-to-roll continuous deposition process. Key factors leading to the attainment of high efficiency cells were discussed. While the terrestrial products have seen applications toward the building integrated systems, the space application is still in its infancy. With a "down to earth" approach and focused effort, we shall reach the goal of providing low-cost, high-quality, and environmentally-friendly a-Si PV to the growing world market. Taking advantage of the high specific power and other superior characteristics of a-Si PV for space application, we shall reach the "final frontier" in the near future.

Acknowledgements

We thank S. R. Ovshinsky and H. Fritzsche for valuable discussions throughout the years, and colleagues at United Solar Systems Corp. (United Solar), in particular, the entire R&D Group, Energy Conversion Devices, Inc., and the National a-Si team members for fruitful collaborations. Funding from the National Renewable Energy Laboratory through the Thin-Film Partnership program over the years is acknowledged; this work is partially supported by subcontract No. ZDJ-2-30630-19. Assistance in manuscript preparation by Sharon Sundquist is appreciated.

References

- [1] J. Yang, A. Banerjee, and S. Guha, *Appl. Phys. Lett.* **70** (1997) 2975.
- [2] S. R. Ovshinsky, *Technical Digest of the International PVSEC-1* (1984) 577.
- [3] M. Izu and T. Ellison, *Solar Energy Materials and Solar Cells* (this volume).
- [4] D. L. Staebler and C. R. Wronski, *Appl. Phys. Lett.* **31** (1977) 292.
- [5] J. Yang, R. Mohr, and R. Ross, *Technical Digest of the International PVSEC-1* (1984) A-IIa-L6.
- [6] J. Yang, K. Lord, S. Guha, and S. R. Ovshinsky, *Mater. Res. Soc. Symp. Proc.* **609** (2000) A15.4.
- [7] J. Yang and S. Guha, *Appl. Phys. Lett.* **61** (1992) 2917.
- [8] J. Yang, R. Ross, R. Mohr, and J. Fournier, *18th IEEE PVSC* (1985) 1519.
- [9] R. Ross, R. Mohr, J. Fournier, and J. Yang, *19th IEEE PVSC* (1987) 327.
- [10] X. Xu, J. Yang, and S. Guha, *23rd IEEE PVSC* (1993) 971.
- [11] S. Guha, J. Yang, P. Nath, and M. Hack, *Appl. Phys. Lett.* **49** (1986) 218.
- [12] A. Banerjee, J. Yang, T. Glatfelter, K. Hoffman, and S. Guha, *Appl. Phys. Lett.* **64** (1994) 1517.
- [13] J. Yang, A. Banerjee, K. Lord, and S. Guha, *2nd World Conf. on Photovoltaic Solar Energy Conversion Proc.* (1998) 387.
- [14] S. Guha, K. L. Narasimhan, and S. M. Pietruszko, *J. Appl. Phys.* **52** (1981) 859.
- [15] J. Yang, X. Xu, and S. Guha, *Mater. Res. Soc. Symp. Proc.* **336** (1994) 687.
- [16] S. Guha, J. Yang, A. Banerjee, B. Yan, and K. Lord, *Solar Energy Materials and Solar Cells* (this volume).
- [17] S. Guha, J. Yang, A. Pawlikiewicz, T. Glatfelter, R. Ross, and S. R. Ovshinsky, *Appl. Phys. Lett.* **54** (1989) 2330.
- [18] J. Yang, R. Ross, T. Glatfelter, R. Mohr, and S. Guha, *PVSEC-4* (1989) 409.
- [19] J. Yang, A. Banerjee, K. Lord, and S. Guha, *28th IEEE PVSC* (2000) 742.
- [20] See, for example, H. Fritzsche, *Annu. Rev. Mat. Res.* **31** (2001) 47.
- [21] A. Banerjee, J. Yang, and S. Guha, *Mater. Res. Soc. Symp. Proc.* **557** (1999) 743.
- [22] S. Guha, J. Yang, A. Banerjee, T. Glatfelter, K. Hoffman, S. R. Ovshinsky, M. Izu, H. C. Ovshinsky, and X. Deng, *Mater. Res. Soc. Symp. Proc.* **336** (1994) 645.
- [23] S. Guha, J. Yang, A. Banerjee, K. Hoffman, and J. Call, *AIP Conference Proceedings* **462** (1998) 88.
- [24] For more information on Uni-Solar products, visit our website at www.uni-solar.com.
- [25] P. Nath, C. Vogeli, K. Jones, A. Singh, I. Garcia, and S. Guha, *28th IEEE PVSC* (2000) 1543.

- [26] S. Guha, J. Yang, A. Banerjee, T. Glatfelter, G. J. Vendura, Jr., A. Garcia, and M. Kruer, *2nd World Conf. on Photovoltaic Solar Energy Conversion Proc.* (1998) 3609.
- [27] S. Guha, J. Yang, A. Banerjee, P. Nath, J. Call, T. Glatfelter, F. J. Boelens, and G. Oomen, *34th Intersociety Energy Conversion Engineering Conference* (1999).
- [28] M. Kagan, V. Nadorov, S. Guha, J. Yang, and A. Banerjee, *28th IEEE PVSC* (2000) 1261.
- [29] K. Beernink, G. Pietka, J. Noch, K. Younan, D. Wolf, A. Banerjee, J. Yang, S. Jones, and S. Guha, *Mater. Res. Soc. Symp. Proc.* **715** (2002) V 6.2.
- [30] K. Beernink, G. Pietka, J. Noch, D. Wolf, A. Banerjee, J. Yang, S. Guha, and S. J. Jones, *29th IEEE PVSC* (2002) 3P2.14.

TABLE I. Characteristics of a-Si/a-Si double-junction cells with different tunnel-junction structures.

Tunnel-junction structure	J_{sc} (mA/cm ²)	V_{oc} (V)	FF	η (%)	Q_{top} (mA/cm ²)	Q_{btm} (mA/cm ²)	Q_{total} (mA/cm ²)	R_s (Ω cm ²)
standard	7.80	1.901	0.752	11.15	7.97	7.80	15.77	15.0
improved	8.06	1.919	0.766	11.85	8.06	8.28	16.34	14.3

TABLE II. Best stabilized efficiency for the top, middle, and bottom component cells achieved at United Solar.

		J_{sc} (mA/cm ²)	V_{oc}	FF	P_{max} (mW/cm ²)
top cell ^{+a}	initial	9.03	1.024	0.773	7.15
	stable*	8.76	0.990	0.711	6.17
middle cell ^{+b}	initial	10.29	0.754	0.679	5.27
	stable**	9.72	0.722	0.600	4.21
bottom cell ^{++c}	initial	12.2	0.631	0.671	5.17
	stable**	11.1	0.609	0.622	4.21

+ solar cells made on stainless steel

++ solar cells made on Ag/ZnO BR

* light soaked under one sun at 50 °C, open circuit

** light soaked under filtered one sun at 50 °C, open circuit

a top cell J-V measured under AM1.5

b middle cell J-V measured under AM1.5 with a $\lambda > 530$ nm filter

c bottom cell J-V measured under AM1.5 with a $\lambda > 630$ nm filter

TABLE III. Highest stable cell efficiencies (active area $\sim 0.25 \text{ cm}^2$) at United Solar for different junction configurations.

		J_{sc}	V_{oc}	FF	η
		(mA/cm ²)	(V)		(%)
a-Si:H single junction	initial	14.65	0.992	0.730	10.6
	stable	14.36	0.965	0.672	9.3
a-Si:H/a-Si:H same gap double junction	initial	7.9	1.89	0.76	11.4
	stable	7.9	1.83	0.70	10.1
a-Si:H/a-SiGe:H dual gap double junction	initial	11.04	1.762	0.738	14.4
	stable	10.68	1.713	0.676	12.4
a-Si:H/a-SiGe:H a-SiGe:H triple junction	initial	8.57	2.357	0.723	14.6
	stable	8.27	2.294	0.684	13.0

Figure Captions

- Fig. 1. Schematic diagram of different cell structures.
- Fig. 2. Quantum efficiency of an a-SiGe:H cell deposited on SS and Ag/ZnO showing the enhancement in J_{sc} due to the back reflector.
- Fig. 3. (a) Initial AM1.5 J-V characteristic and (b) corresponding quantum efficiency of a triple-junction a-Si alloy solar cell that stabilized to 13% efficiency after light soaking.
- Fig. 4. Schematic diagram of a roll-to-roll a-Si alloy triple-junction solar cell processor.
- Fig. 5. Block diagram of the module fabrication process.
- Fig. 6. A lightweight, foldable a-Si PV product for charging batteries.
- Fig. 7. An example of an esthetically pleasing building integrated a-Si PV product on top of the left rectangular metal roof.
- Fig. 8. Initial AM0 J-V characteristic of a triple-junction a-Si alloy solar cell of area 412 cm^2 , showing an efficiency of 9% and a specific power of 1256 W/kg measured at NASA Glenn Research Center.

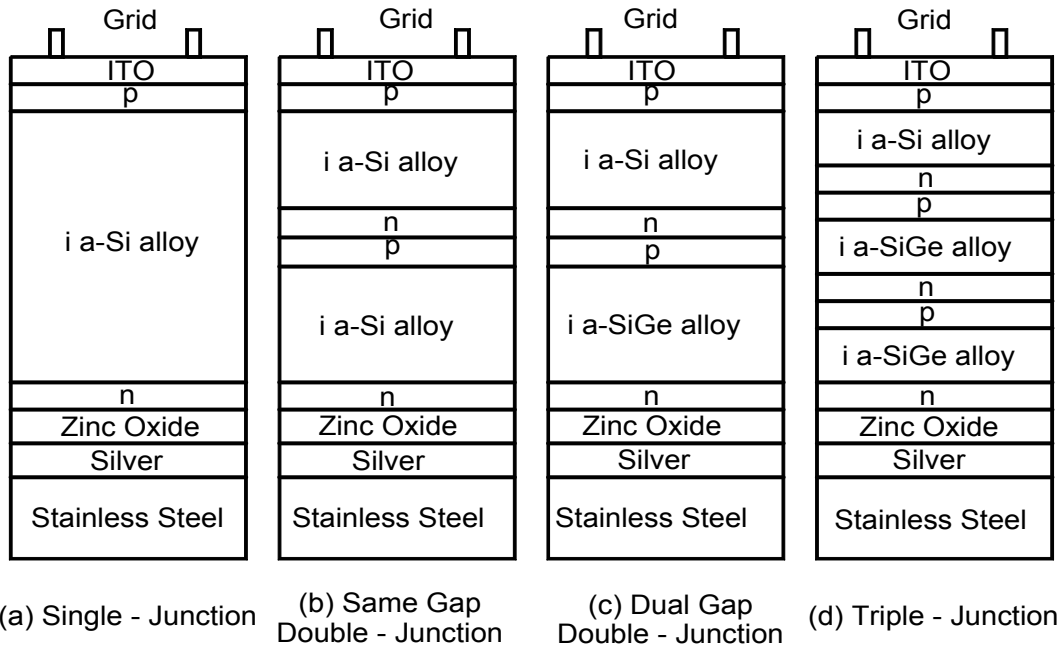


Fig. 1. Yang et al.

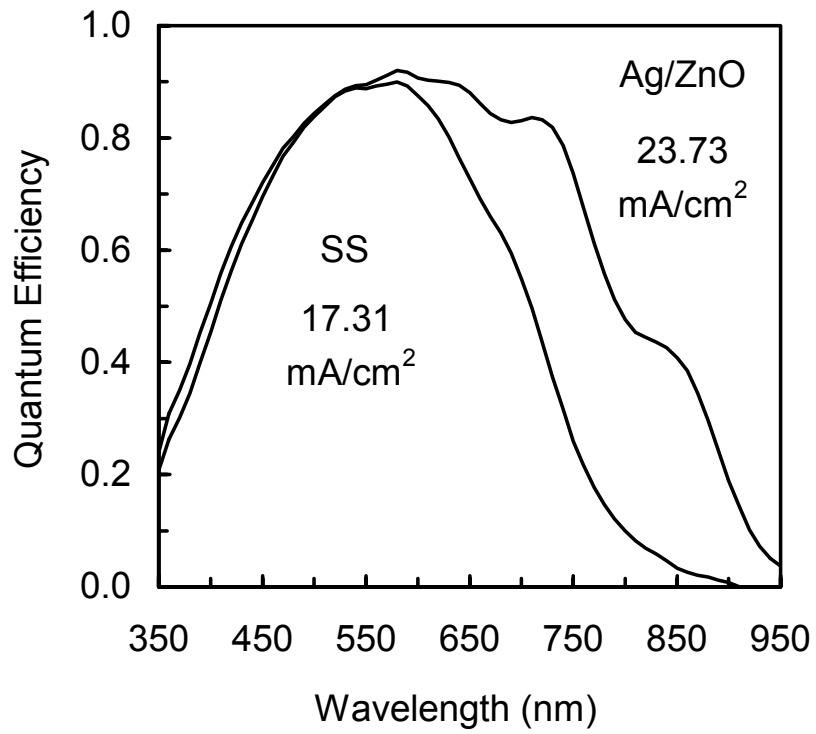


Fig. 2. Yang et al.

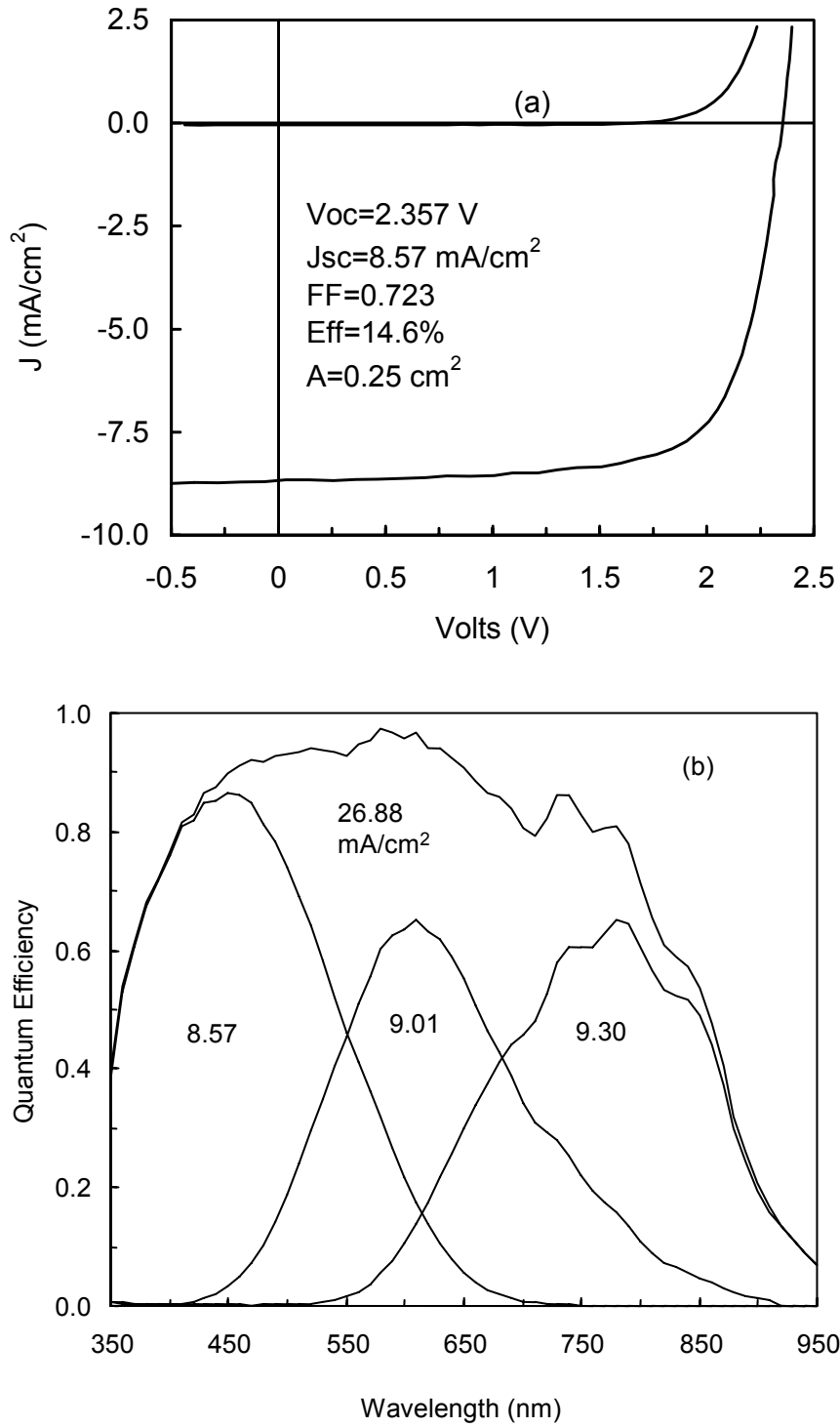


Fig. 3. Yang et al.

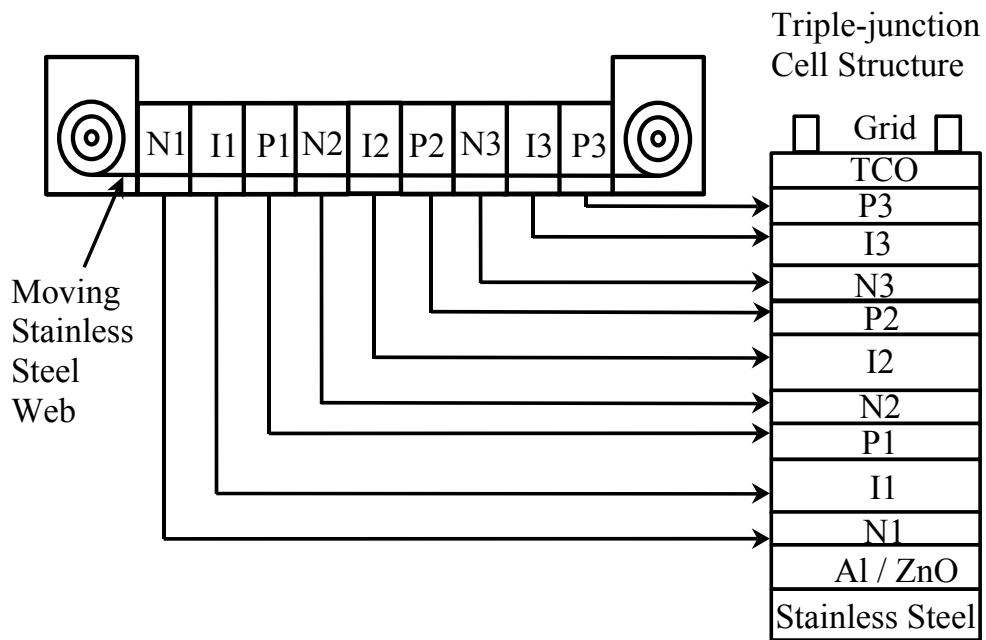


Fig. 4. Yang et al.

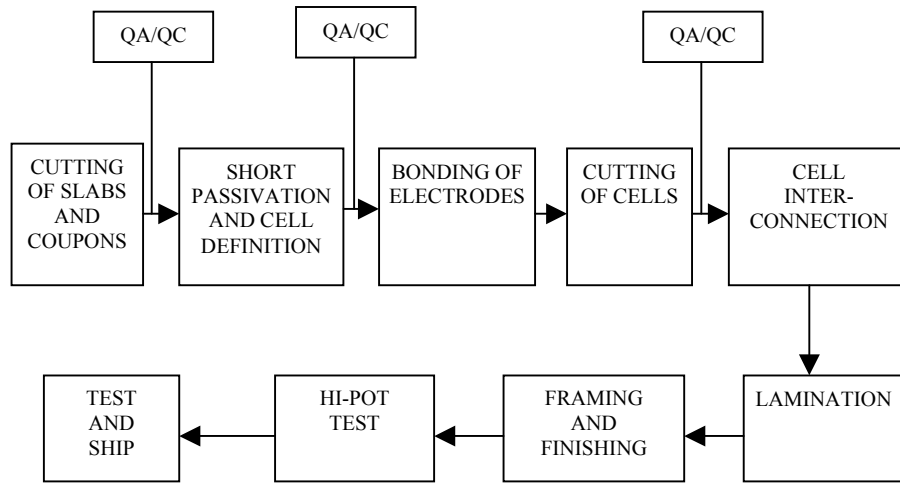


Fig. 5. Yang et al.



Fig. 6. Yang et al.



Fig. 7. Yang et al.

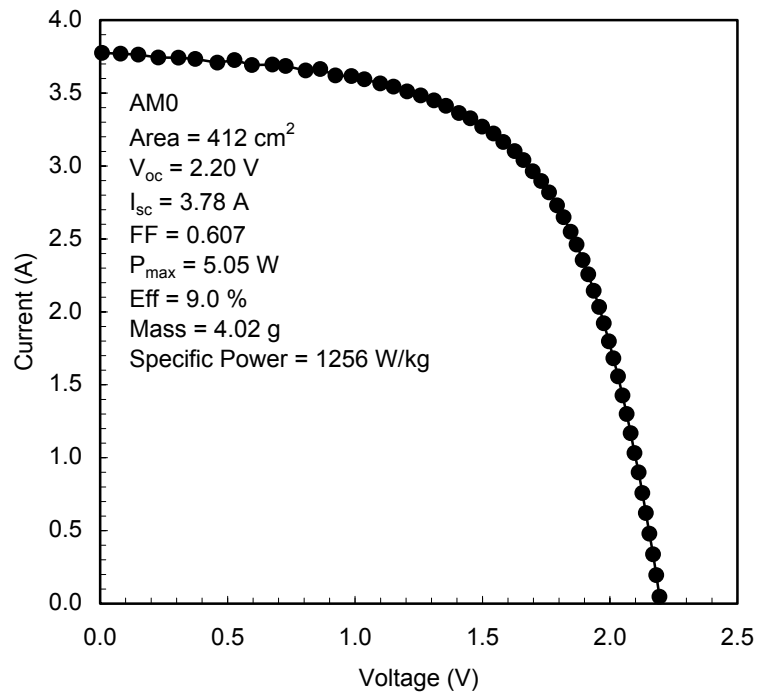


Fig. 8. Yang et al.